ELSEVIER

Surface Science 429 (1999) 229–236

surface science

www.elsevier.nl/locate/susc

XPD and STM investigation of hexagonal boron nitride on Ni(111)

W. Auwärter, T.J. Kreutz, T. Greber *, J. Osterwalder

Physik-Institut, Universität Zürich, Winterthurerstrasse 190, CH-8057 Zürich, Switzerland

Received 4 December 1998; accepted for publication 26 February 1999

Abstract

Monolayers of hexagonal boron nitride have been grown by the reaction of benzene-like borazine $(BN)_3H_6$ with Ni(111) at 1050 K. The resulting layers are analyzed by means of Si Kα excited N 1s and B 1s X-ray photoelectron diffraction (XPD) and scanning tunneling microscopy (STM). STM shows large terraces without defects and resolves two different atomic species that are commensurate with Ni(111). From XPD it is found that the system discriminates fcc from hcp adsorption sites, that the h-BN layer is corrugated and that nitrogen terminates the surface. The B–N corrugation is determined quantitatively by *R*-factor analysis between single scattering cluster calculations and experiment. The results are discussed in connection with an existing LEED analysis on the same system [Y. Gamou, M. Terai, A. Nagashima, C. Oshima, Sci. Rep. RITU A 44 (1997) 211].

Keywords: Scanning tunneling microscopy; Surface structure; X-ray photoelectron diffraction

1. Introduction

Boron nitrides are a class of materials with promising properties [2]. They are thermally stable, chemically inert and insulating. Stoichiometric boron nitrides are isoelectronic to carbon compounds. Correspondingly, analogous forms such as graphite-like hexagonal boron nitride (h-BN), diamond-like cubic boron nitride (c-BN), fullerenes or nanotubes exist or are predicted.

In the case of hexagonal boron nitride the difference in electronegativity between nitrogen and boron induces ionicity and electrons are transferred from boron to nitrogen. This causes — in contrast to graphite — h-BN to become insulating with a band gap around 5 eV [3].

Recently, Nagashima et al. produced and analyzed high quality single h-BN layers on various (111) transition metal surfaces [4]. They used benzene-like borazine $(BN)_3H_6$ that reacts with hot transition metal surfaces under the formation of hydrogen and h-BN. Since the reaction rate drops by more than two orders of magnitude after completion of the first h-BN plane, it is an excellent way to produce well-defined surfaces. Among the (111) transition metal surfaces Ni has the lowest lattice misfit with h-BN. On Ni(111) the layers grow commensurate and the misfit of -0.4% is compensated by corrugation and a nitrogen terminated surface [1]. The electronic [5] and the vibronic structure [6] indicate a strong h-BN bond to Ni(111) but — in contrast to single graphite layers — no hybridization of BN π states with the d-band of the substrate is found.

In this paper we show atomically resolved scan-

* Corresponding author. Fax: +41-1-635-5704.
E-mail address: greber@physik.unizh.ch (T. Greber)

0039-6028/99/$ – see front matter
PII: S0039-6028(99)00381-7

ning tunneling microscopy (STM) data from h-BN single layers on Ni(111). They indicate large terraces, defect-free films, and that tunneling is not inhibited across such layers. This provides a firm basis for the subsequent X-ray photoelectron diffraction (XPD) investigation. The data confirm the structural model of Gamou et al. [1]. From comparison between experiments and single scattering cluster calculations (SSC) the corrugation is determined quantitatively. Our corrugation value is, however, lower than that of the previous LEED study [1].

2. Experimental

The experiments were done in two different ultra-high vacuum (UHV) chambers. All data are taken on the same Ni(111) crystal at room temperature. Photoemission was performed in a modified VG ESCALAB 220 spectrometer [7]. The STM experiments were carried out with a VP2 scanning probe from Park Scientific Instruments. The microscope was mounted in a stand-alone system on a home-made table with three legs and an air damping system. The UHV chamber is pumped by a wide range turbomolecular pump, an ion pump and a home-made cerium getter pump. At a base pressure below 5×10^{-11} mbar, atomic resolution is achieved on Ni(111) with the turbomolecular pump in the standby mode. NaOH etched W tips were used. The lateral scanner was calibrated on an atomically resolved gold sample.

The Ni(111) single crystal has been cleaned by repeated cycles of Ar^+ bombardment (0.8 kV), exposure to 30 L O_2 and subsequent annealing to 1000 K [8]. The sample cleanliness was verified by X-ray photoelectron spectroscopy (XPS, less than 1% carbon contamination) or by STM.

The hexagonal boron nitride layers were prepared according to the recipe given by Nagashima et al. [9]. In this procedure the Ni(111) surface is kept at 1070 K and exposed to benzene-like borazine $(BN)_3H_6$ that reacts under the formation of hydrogen to a monolayer of stoichiometric hexagonal boron nitride. As soon as the first monolayer is complete the reaction rate drops by more than two orders of magnitude. Perfect single layers of h-BN on Ni(111) can therefore be produced. The small lattice misfit between Ni(111) and h-BN of -0.4% favors the formation of commensurate layers. The h-BN layers that are discussed in this paper result after exposure to 60 L of borazine on Ni(111) at 1050 K. The exposure is determined without correction for the ionization probability from the pressure reading of the ion gauge.

In order to get a good signal-to-noise ratio in the XPD data, the angular resolution was set to $5.0\pm0.5^\circ$ FWHM and the energy resolution to 1.2 eV FWHM. XPD measurements of full hemispherical B 1s and N 1s intensity patterns typically take one day. After these measurements no change in the XP spectra was found. Each XPD plot presented in the following shows the intensity in a linear grayscale of a particular core level (B 1s or N 1s) along typically 5000 emission angles into the hemisphere above the surface. The emission angles are stereographically projected, i.e. plotted with radii proportional to $\tan(\theta/2)$ where the center of the plot corresponds to normal and the circumference to grazing emission [10]. Data are recorded from grazing ($\theta=88^\circ$) to normal ($\theta=0^\circ$) emission. In order to account for the lower emission intensity parallel to the surface, the individual azimuthal scans have been normalized by the average intensity at this particular polar emission angle. The anisotropy A is defined as $A=(I_{max}-I_{min})/I_{max}$.

3. Results and discussion

3.1. STM

Fig. 1 shows STM pictures of the surface after formation of a h-BN layer on Ni(111). Fig. 1a displays a large area topography scan (1 nA, +100 mV) of atomically flat terraces separated by steps with a height of about 2 Å. It indicates that the h-BN layers grow flat and perfect. Since the average terrace width on pristine Ni(111) (not shown) is by more than a factor of two smaller, it is inferred that the formation process of the h-BN layer involves a flattening of the substrate. The Ni(111) and the h-BN on Ni(111) surfaces can be further distinguished by their different behavior towards residual gases or metal vapor. In Fig. 1b a picture with atomic resolution from a h-BN layer

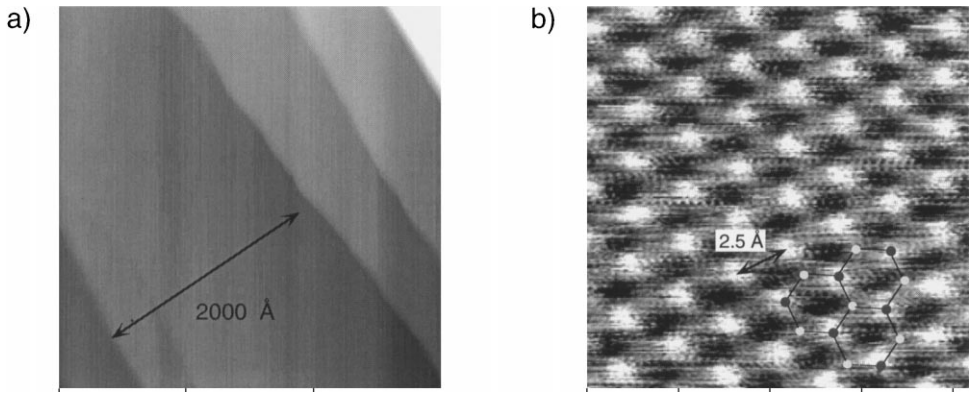

Fig. 1. STM pictures of a h-BN layer on Ni(111). (a) Large area topography scan showing atomically flat terraces separated by atomic steps. (b) The atomically resolved picture clearly shows two hexagonal lattices with a lattice constant of 2.5 ± 0.1 Å that form a honeycomb pattern.

on Ni(111) is shown. This current image ($0.2 < I_t < 0.5$nA) was recorded at constant height with a W tip at $+4.8$ mV bias voltage. It clearly indicates two hexagonal Bravais lattices that form a honeycomb pattern. The observed lattice constant of 2.5 ± 0.1 Å corresponds to that of the Ni(111) substrate (2.49 Å). These findings stand for a well-ordered surface with two distinct atomic species. At the moment we are not able to make a clear assignment of the two atomic species and sites. Formally, h-BN is an insulator that should not contribute to the tunneling current at such low tunneling voltages. It is, nevertheless, not evident whether the pictures represent electron current from Ni or from B and N atoms. This is not clear even if we take the structure as determined by Gamou et al. [1], where nitrogen terminates the surface on on-top sites and where boron sits on fcc hollow sites. The bright spots with the highest conductance may correspond to nitrogen or top-layer nickel atoms and those with lower conductance to boron (on fcc) or second-layer nickel atoms (on hcp sites). Only with the absolute orientation of the Ni(111) surface in the microscope will it be possible to discriminate between fcc and hcp sites, and the puzzle of which atoms are seen may be solved.

3.2. XPS and XPD direct interpretation

XPS and XPD have been employed for the determination of the chemical composition and the structure of the h-BN monolayers on Ni(111). In Fig. 2 the Si Kα ($\hbar\omega = 1740$ eV) excited XP spectrum at normal emission of one monolayer of h-BN on Ni(111) is shown. It displays the main constituents boron, nitrogen and nickel. The insets highlight the B 1s and the N 1s spectra that were recorded in the angle scanned photoelectron diffraction data (Fig. 3). From the B 1s, the N 1s and the Ni 3s photoelectron intensities we get after normalization with the corresponding photoemission cross-sections a composition of $8.4 \pm 0.3\%$ B, $8.9 \pm 0.4\%$ N, and $82.7 \pm 4\%$ Ni. With an electron attenuation length of 15 Å these intensities are

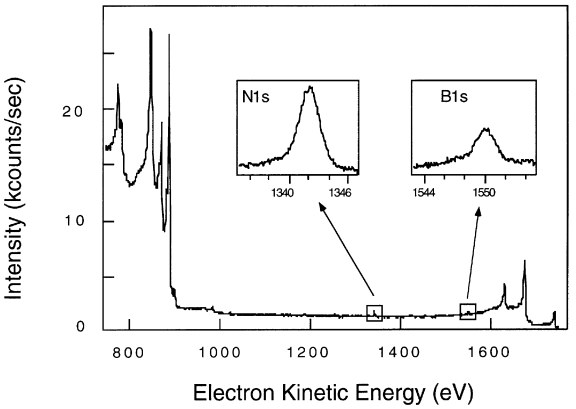

Fig. 2. Si Kα excited normal emission photoemission spectrum of one monolayer of h-BN on Ni(111). The insets show the B 1s and the N 1s spectrum, respectively.

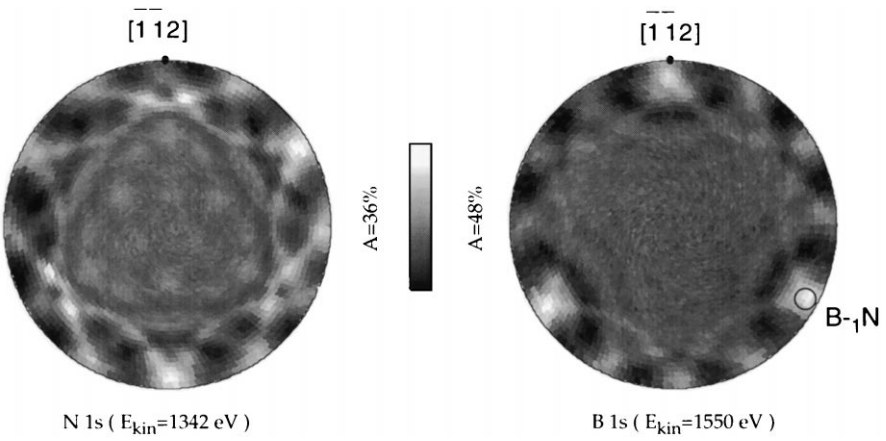

Fig. 3. X-ray photoelectron diffraction patterns of h-BN on Ni(111). (a) N 1s emission ($E_{kin}=1342$ eV) and (b) B 1s ($E_{kin}=1550$ eV) emission. One ($B_{-1}N$) forward scattering peak is indicated as well.

compatible with a film thickness of one monolayer of stoichiometric h-BN.

Fig. 3 depicts the B 1s and the N 1s photoelectron diffraction data from one monolayer of h-BN on Ni(111). The absolute azimuthal orientation as indicated with the $[\bar{1}\bar{1}2]$ direction is found from measurements of the Ni 3s diffraction pattern (not shown). First it will be demonstrated how much straightforward information on the structure may be drawn directly from these data. The principal scattering mechanism for photoelectron energies above 500 eV is forward focusing. This means that a photoelectron wave that is emitted from a particular atom scatters mainly along neighbor directions. Furthermore, circular diffraction features centered on cones along those axes contribute to the diffraction patterns. The N 1s and the B 1s diffraction patterns in Fig. 3 are three-fold symmetric and differ in their anisotropies (36% for N 1s and 48% for B 1s). If the first Ni layer only were to determine the orientation of the BN layer, two six-fold diffraction patterns that correspond to two oppositely oriented honeycomb domains would be expected. The observed three-fold symmetry indicates the decisive role of the second Ni layer for the layer formation, since the system discriminates fcc from hcp adsorption sites. Furthermore, the differences in N 1s and B 1s diffraction patterns indicate a corrugation of the BN layer. If the layers were flat we would expect — up to rotation by 180° — similar diffraction patterns for boron and nitrogen emission. The fact that the anisotropy in the B 1s diffraction pattern is larger than that in the N 1s pattern indicates that the B 1s photoelectrons undergo forward scattering into the hemisphere above the surface, while there is no such forward scattering for N 1s photoelectrons. In the N 1s diffraction patterns barely visible 'forward scattering'-like features along the $\langle 110 \rangle$ and the $\langle 100 \rangle$ directions indicate Ni(111) substrate diffraction peaks that partly survive the background subtraction procedure. These features are artifacts and it is concluded that nitrogen atoms terminate the surface.

From the position of the forward scattering maxima in the B 1s diffraction pattern at a polar angle of 86° (see Fig. 3) a corrugation angle of 4° is deduced. For polar angles $<80°$ no forward scattering peaks are observed. This indicates that there is no ordered structure above the BN layer. Together with the findings from the STM experiments it can therefore be concluded that the h-BN layer terminates the surface. In order to determine the corrugation height the distance between the emitter and the scatterer has to be known. This is given by the electron wavelength, the opening angle of the first order diffraction cone and the particular scattering phase shift for this atom at this energy and angle [10].

In Fig. 4 the N 1s diffraction pattern of Fig. 3a

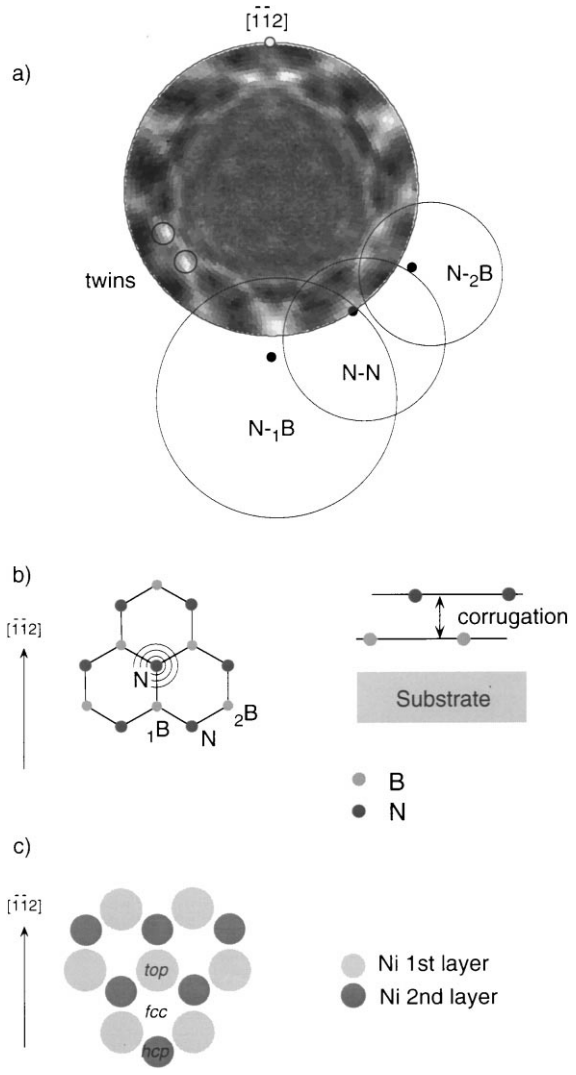

Fig. 4. N 1s X-ray photoelectron diffraction pattern of h-BN on Ni(111). (a) N 1s emission pattern with circles that highlight the first order diffraction cones (N–$_1$B), (N–N) and (N–$_2$B). The twin peaks result from constructive interference between two diffraction cones. (b) Corresponding honeycomb layer structure. (c) Ni(111) substrate where the absolute orientation [$\bar{1}\bar{1}$2] is known from Ni 3s XPD. On top, fcc and hcp high symmetry adsorption sites are indicated as well.

is shown again. Circles highlight the first order interference cones that are mapped in the stereographic projection as circles. Note that the centers of the circles do not correspond to the projections of the cone axes. This is a consequence of the nonlinear mapping function [tan(θ/2)] for the stereographic projection. As can be inferred from Fig. 4, the circle N–$_1$B indicates the nearest neighbor first order scattering cone, the circle N–N that of the next nearest neighbor and the circle N–$_2$B that of the third coordination shell around the emitter. From the first interference cone the N–$_1$B direction is found to point 4° below the surface. This is consistent with the opposite B–$_1$N direction 4° above the surface.

In order to get a value for the corrugation the angle and a length has to be known. For the cone in the [11$\bar{2}$] azimuth with an opening angle of 37° and an electron energy of 1342 eV ($k=19$ Å^{-1}) we thus get an emitter scatterer distance $d=2\pi/k[1-\cos(\theta)]$ [10] of 1.6 ± 0.2 Å. In this estimation the scattering phase shift of the scattering atom is not included and thus the quoted value is an upper limit. With the known commensurability (from STM) and the N–$_1$B distance of 1.6 ± 0.2 Å we can thus set the horizontal N–$_1$B distance equal to $a_0/\sqrt{3}$ where a_0 is the Ni nearest neighbor distance (2.49 Å). With the corrugation angle of 4° we then get from trigonometric considerations a corrugation of 0.1 Å.

In Fig. 4 it can be seen as well that the next nearest neighbor N–N scattering cone axis lies in the surface plane and that the first order diffraction cone has — as expected — a smaller opening angle than the N–$_1$B nearest neighbor first order diffraction cone. The cone N–$_2$B of the third coordination shell around the emitter indicates a cone axis and opening angle that are compatible with the larger emitter scatterer distance and the corrugation found above.

In the N 1s diffraction pattern high intensity spots that might be interpreted as forward scattering peaks can be seen as well. Such peaks have been observed before, e.g. in the Na on Al(001) system [11]. They may appear whenever two diffraction cones cross each other and signify particular directions in k-space. If the scattering process is coherent, as e.g. expected from a single emitter, we expect a superposition of amplitudes in these directions and thus a squared amplification of diffraction intensity. The twin peaks in the N 1s diffraction pattern do indeed indicate a nonlinear pile-up of diffraction intensity and suggest

the twin features to be caused by a coherent emission and scattering process. All these findings are consistent with a corrugated honeycomb structure of the boron nitride on top of the Ni(111) substrate (see Fig. 4b). Now the lateral configuration of the h-BN with respect to the underlying Ni unit cell shall be addressed.

From the commensurate structure of h-BN on Ni(111) it can be expected that the nitrogen and the boron atoms occupy high symmetry sites in the Ni(111) unit cell. Gamou et al. [1] investigated six lateral configurations that correspond to the arrangement of two different atoms (nitrogen and boron) on three different sites (on top, fcc and hcp). The fcc and hcp sites are the two three-fold hollow sites. Below the fcc site no atom is found in the second substrate layer (see Fig. 4c). One of the configurations (N,B) ∈ {(fcc,hcp), (hcp,fcc), (hcp,top), (top,hcp), (top,fcc), (fcc,top)} is therefore possible. The XPD results give an absolute orientation of the B–N direction and thus reduce the six structural models to three: (N,B) ∈ {(fcc,hcp), (hcp,top), (top,fcc)}. The LEED analysis of Gamou et al. [1] is consistent with this subset and favors the configuration with nitrogen on top and boron on fcc sites. In principle XPD may also discriminate between the three remaining models. Then backscattering features from the Ni substrate have to be observed in the N 1s or B 1s diffraction patterns. Recently it was demonstrated for the case of oxygen on rhodium [12,13] that such patterns may indeed be observed even for electron energies as high as 720 eV. In the present study we did not, however, find significant indications for the adsorption site of N or B within the Ni(111) unit cell. The reason for this might be the higher temperature and the correspondingly larger Debye–Waller factors and the lower backscattering amplitudes from Ni at 1550 and 1342 eV compared with Rh at 723 eV.

3.3. Quantification of the B–N corrugation by SSC calculations

In order to quantify the structural parameters we performed SSC calculations within the Rehr Albers formalism [14,15]. The h-BN layers provide a self-consistency test, since both nitrogen and

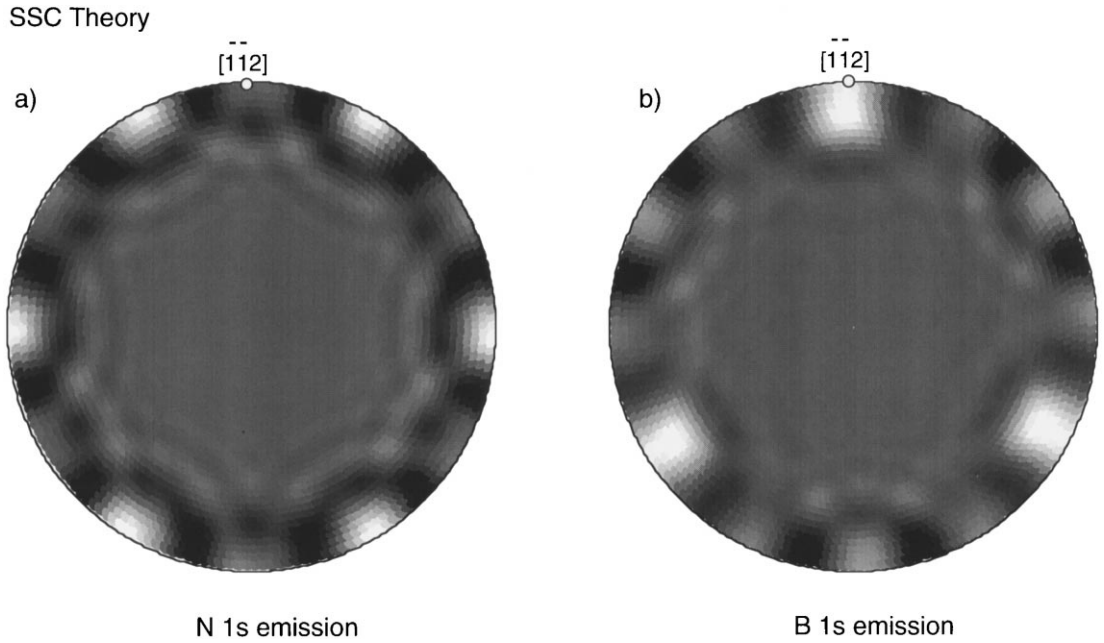

Fig. 5. Single scattering X-ray photoelectron diffraction calculations of h-BN on Ni(111) for a corrugation of 0.1 Å. (a) N 1s (E_{kin} = 1342 eV) emission. (b) B 1s (E_{kin} = 1550 eV) emission.

boron emission are measured and simulated independently while the same corrugation from nitrogen and boron emission is expected. The calculations were performed on single h-BN layer clusters with 13 atoms (like in Fig. 4b). The lateral lattice constant was kept commensurate with Ni(111) at 2.49 Å. The inner potential ($V_0 =$ 10 eV) and the electron mean free path ($\Lambda = 11$ Å) were kept constant. The *R*-factor was defined as $R^2 = \Sigma(I_{exp} - I'_{theo})^2$, where ΣI_{exp} and $\Sigma I'_{theo}$ were normalized to *n*, the number of data points. I'_{theo} was determined from I_{theo} by imposing the same anisotropy as that of the experiment.

In Fig. 5 the calculated N 1s and B 1s diffraction patterns for a B–N corrugation of 0.1 Å are shown. This value is close to the *R*-factor minima. The best agreement between experiment (Fig. 3) and theory yields *R*-factors of 0.0021 for N 1s emission and 0.0030 for B 1s emission. The single scattering calculations shown in Fig. 5 reproduce all features of the experimental diffraction patterns in Fig. 3. They indicate, however, shortcomings such as the well-known overestimation of forward scattering [16]. This is best seen in the N 1s calculation where the forward scattering peaks of the six in-plane nitrogen next-nearest neighbors dominate the scattering pattern. The Debye–Waller factors $W = \exp\{-2k^2[1-\cos(\theta)]u^2\}$ were optimized with respect to the mean square vibrational displacement u^2. The best values for u^2 are 0.011 ± 0.005 Å^2 for N 1s and 0.007 ± 0.002 Å^2 for B 1s emission. Although fitting the Debye–Waller factors lowers the *R*-factor minima by about 30%, they do not affect the minima positions of the corrugation significantly. For the corrugation, which is the vertical outward displacement of the nitrogen layer relative to the boron layer, a value of 0.11 ± 0.07 Å from the N 1s emission and 0.03 ± 0.05 Å from the B 1s emission is found. Within the error bars, which were determined from the corrugation values with an *R*-factor 5% above the minimum, these two values agree and a mean corrugation value of 0.07 ± 0.06 Å is deduced.

In principle the value for the corrugation should be independent of the emitter species. The reason for the remaining discrepancy between the two *R*-factor minima may have various reasons. Multiple scattering, the ionicity of the layer or the fact that Debye–Waller factors do not sufficiently account for all effects of thermal vibrations. A concept — beyond Debye–Waller factors — is that of the split positions [17] where the geometry of the atom is varied. In a study of Yb on Al(001) it was shown that this concept improves the *R*-factors of XPD structural determinations as well as those of the complementary LEED analysis on the same system [18]. The reason for the implementation of the thermal distortion in real space is that the forward scattering is not altered by Debye–Waller factors [$W(\theta = 0^\circ) = 1$]. As long as the forward scattering cones are much wider than the cones that are imposed due to the vibrational displacement, this should not be very important. In our case we find upon introduction of a reasonable vibrational distortion of the equilibrium sites that the *R*-factor minima positions (corrugation values) of the boron and the nitrogen emission patterns approach each other. However, the discrepancy between the boron- and nitrogen-derived corrugation does not disappear completely and, more importantly, the *R*-factors do not improve.

4. Conclusions

The high quality of h-BN layers on Ni(111) enables a precise determination of a structural model. Our findings are consistent with the LEED analysis of Gamou et al. [1]. XPD is rather sensitive to the B–N corrugation. This corrugation has e.g. to be known in order to get a measure of the stress in the layer or of how much sp^3 character mixes into the planar sp^2 bonds. Our corrugation value of 0.07 ± 0.06 Å is slightly lower than that of the previous LEED study, 0.18 Å [1]. Due to weak backscattering from nickel the presented boron and nitrogen XPD data are, however, not sensitive to the lateral arrangement of the h-BN honeycomb in the unit cell of the substrate.

In conclusion, it is found that perfect single h-BN layers may be grown and well characterized on Ni(111). This system promises to be a good candidate substrate for the study of electron coupling between two metals and their Fermi surfaces across a thin insulator.

Acknowledgements

We are grateful to Professor Nöth for the production of borazine and for the indispensable support of H. Keller, W. Deichmann, B. Zaugg and B. Schmid.

References

[1] Y. Gamou, M. Terai, A. Nagashima, C. Oshima, Sci. Rep. RITU A 44 (1997) 211.
[2] S.P.S. Arya, A. D'Amico, Thin Solid Films 157 (1988) 267.
[3] A. Catellani, M. Posternak, A. Baldereschi, A.J. Freeman, Phys. Rev. B 36 (1987) 6105.
[4] A. Nagashima, N. Tejima, Y. Gamou, T. Kawai, C. Oshima, Surf. Sci. 357/358 (1996) 307.
[5] A. Nagashima, N. Tejima, Y. Gamou, T. Kawai, C. Oshima, Phys. Rev. Lett. 75 (1995) 3918.
[6] E. Rokuta, Y. Hasegawa, K. Suzuki, Y. Gamou, C. Oshima, Phys. Rev. Lett. 79 (1997) 4609.
[7] T. Greber, O. Raetzo, T.J. Kreutz, P. Schwaller, W. Deichmann, E. Wetli, J. Osterwalder, Rev. Sci. Instrum. 68 (1997) 4549.
[8] T.J. Kreutz, T. Greber, P. Aebi, J. Osterwalder, Phys. Rev. B 58 (1998) 1300.
[9] A. Nagashima, N. Tejima, Y. Gamou, T. Kawai, C. Oshima, Phys. Rev. B 51 (1995) 4606.
[10] J. Osterwalder, T. Greber, A. Stuck, L. Schlapbach, Phys. Rev. B 44 (1991) 13764.
[11] R. Fasel, P. Aebi, J. Osterwalder, L. Schlapbach, R.G. Agostino, G. Chiarello, Phys. Rev. B 50 (1994) 14516.
[12] T. Greber, J. Wider, E. Wetli, J. Osterwalder, Phys. Rev. Lett. 81 (1998) 1654.
[13] J. Wider, T. Greber, E. Wetli, T.J. Kreutz, P. Schwaller, J. Osterwalder, Surf. Sci. 417 (1998) 301.
[14] J.J. Rehr, R.C. Albers, Phys. Rev. B 41 (1990) 8139.
[15] D.J. Friedman, C.S. Fadley, J. Electron Spectrosc. Relat. Phenom. 51 (1990) 689.
[16] C.S. Fadley, in: R.Z. Bachrach (Ed.), Synchrotron Radiation Research: Advances in Surface Science, Plenum, New York, 1989, Chapter 9.
[17] H. Over, W. Moritz, G. Ertl, Phys. Rev. Lett. 70 (1994) 315.
[18] R. Fasel, M. Gierer, H. Bludau, P. Aebi, J. Osterwalder, L. Schlapbach, Surf. Sci. 374 (1997) 104.